Received: 2 December 2019 | Revised: 26 June 2020 | Accepted: 26 June 2020

DOI: 10.1002/met.1940

RESEARCH ARTICLE

Meteorological Applications RMetS

Improved estimation of global solar radiation over rugged terrains by the disaggregation of Satellite Applications Facility on Land Surface Analysis data (LSA SAF)

Luca Fibbi[1,2] | **Fabio Maselli**[1] | **Maurizio Pieri**[1]

[1]Institute of BioEconomy of National Research Council (IBE-CNR), Sesto Fiorentino, Italy

[2]LaMMA Consortium, Sesto Fiorentino, Italy

Correspondence
Luca Fibbi, Institute of BioEconomy of National Research Council (IBE-CNR), Via Madonna del Piano 10, 50019 Sesto Fiorentino, Firenze, Italy.
Email: fibbi@lamma.rete.toscana.it

Abstract

This paper presents a new method to predict global solar radiation over irregular terrain, named Estimation of global solar RADiation (ERAD). The method is based on the disaggregation of Satellite Applications Facility on Land Surface Analysis (LSA SAF) data using a digital elevation model and is applied in Italy with a time step of 1 min and a spatial resolution of 200 m. A quantitative assessment of ERAD is performed in comparison with three other standard methods (Mountain Microclimate Simulation Model [MTCLIM], LSA SAF and Copernicus Atmosphere Monitoring Service [CAMS]) using measurements taken in 43 stations located in Italy or in the surrounding countries, in the years 2005–2016. Such assessment concerns the irradiance incoming on a horizontal surface, which is measured by ground radiation sensors and is summarized by means of four accuracy statistics (i.e. mean absolute error [MAE], root mean square error [RMSE], coefficient of determination [R^2] and mean bias error [MBE]). Overall, the average daily global solar radiation estimates obtained by ERAD have RMSE and R^2 about 25 $W \cdot m^{-2}$ and 0.943, respectively. These statistics are similar to those of LSA SAF and better than those of CAMS and, above all, MTCLIM. The bias analysis by elevation ranges shows a slight ERAD overestimation over plains and hills and a slight underestimation over mountains. An additional qualitative assessment shows how the ERAD radiation estimates are more spatially detailed than those of the other methods and are redistributed on inclined surfaces consistently with expectations.

KEYWORDS

DEM, disaggregation, global solar radiation, topographic correction

1 | INTRODUCTION

Downwelling Surface Shortwave radiation Flux (DSSF) is the solar irradiance reaching the Earth's surface per unit of time and area (Geiger *et al.*, 2008a). The solar flux, consisting predominantly of ultraviolet–visible and near-infrared (300–4,000 nm) radiation, affects the weather, the climate and most biological processes in terrestrial and marine ecosystems. Therefore, solar radiation is a crucial factor in global warming mechanisms, glacier

retreat, water resource and carbon budgeting (Wild, 2016). In addition, the prediction of solar radiation is decisive to estimate evapotranspiration (Aguilar *et al*., 2010), to predict crop and forest yield (Chirici *et al*., 2016) and for numerous solar energy applications such as photovoltaic systems (Demain *et al*., 2013).

Outside the atmosphere, the solar flux is almost constant and is referred to as solar constant (I_0). The solar flux, before reaching the Earth's surface, interacts with atmospheric constituents and is partially reduced by the phenomena of scattering, absorption and reflection. In clear sky conditions, the atmospheric transmittance mainly depends on water vapour and aerosol characteristics (Lefèvre *et al*., 2013). Instead, in cloudy or partially cloudy sky conditions, the prevailing factors are the optical and physical properties of clouds (Oumbe *et al*., 2009). At ground level, the incoming solar radiation depends on various astronomical and geographical factors including the terrain characteristics (elevation, slope and aspect), which are usually derived from a digital elevation model (DEM). In morphologically complex areas, the grid resolution of the DEM is a factor to consider with due attention, since it affects the estimation accuracy of solar radiation (Huang and Zhao, 2017).

The global solar radiation (I_g) that reaches the surface can be split into direct or beam (I_b), diffuse (I_d) and reflected (I_r) components (Iqbal, 1983) and can be measured by specific sensors (e.g. pyranometers) at weather stations. However, the stations that measure solar radiation are few because of the high cost of sensor installation and maintenance. One of the most famous solar radiation station networks is the World Radiation Data Centre (WRDC: http://wrdc.mgo.rssi.ru) - World Meteorological Organization (WMO) consisting of about 1,600 stations distributed all over the globe. These stations often collect solar radiation in the form of daily or monthly averages but usually show low accuracy and reliability. An exception is represented by the World Radiation Monitoring Center (WRMC) – Baseline Surface Radiation Network (BSRN) (Driemel *et al*., 2018), although there are only 64 and 11 stations over the globe and in the European area, respectively. To overcome the problem of the absence of stations, many indirect methods have been developed based on the correlation between solar radiation and other more easily measurable meteorological or geographical parameters, such as sunshine duration (Suehrcke *et al*., 2013). A typical indirect model is the Mountain Microclimate Simulation Model (MTCLIM) proposed by Thornton and Running (1999) which essentially uses daily temperature range and rainfall observations to estimate incoming solar radiation.

Among the most common methods for estimating solar radiation are those based on meteorological satellites, such as the Meteosat Second Generation (MSG). Geostationary satellites allow the diurnal cycle of solar radiation, or of cloudiness, to be captured due to the high temporal scanning frequency of the acquired images (15 min for MSG) (Journée and Bertrand, 2010). Conversely, the drawbacks of these satellite data are due to low spatial resolution (5 km in the Italian area) and to the consequent poor accuracy in rugged areas.

Classically, the methods to retrieve DSSF from satellite data can follow three main schemes: empirical, physical and semi-empirical (Sengupta *et al*., 2015). Empirical models are based on statistical relationships between the information derived simultaneously from satellite data and ground observations (Tarpley, 1979). Physical approaches use satellite data to solve radiative transfer models (RTMs). These last methods are computationally more expensive and require a detailed and always updated knowledge of the optical properties of the atmosphere (Urraca *et al*., 2017). A series of methods, adopted by many researchers and referred to as Heliosat methods, have evolved towards a semi-empirical, or hybrid, approach. From the first version of the Heliosat method (Cano *et al*., 1986) various improvements were proposed in successive versions, characterized by increasing numbers (Heliosat-1, Beyer *et al*., 1996; Heliosat-2, Rigollier *et al*., 2004; Heliosat-3, Schroedter-Homscheidt *et al*., 2006). All these methods use physical models to describe, in cloudless conditions, the interaction of solar radiation with gases and aerosols in the atmosphere, while satellite-derived data are used to retrieve the cloudiness conditions empirically. Another semi-empirical approach is implemented by the European Organization for the Exploitation of Meteorological Satellites (EUMETSAT) – Satellite Applications Facility on Land Surface Analysis (LSA SAF; Trigo *et al*., 2011). The LSA SAF service provides, amongst others, DSSF products derived from MSG data. In this case, the empirical observations are related both to the presence and optical characteristics of the clouds and to the land surface albedo (Geiger *et al*., 2008a; 2008b).

In the last few years, many semi-empirical methods tend to include more physical descriptions. The convergence to physical methods is feasible due to both the improvements obtained in the RTM calculation times by using a series of discrete pre-calculated solutions saved in look-up tables and the higher availability of ancillary information related to the physical properties of the atmosphere (Urraca *et al*., 2017). An example of these methods is the new version of Heliosat, referred to as Heliosat-4, based on a library of RTMs and distributed by the Copernicus Atmosphere Monitoring Service (CAMS) (Qu *et al*., 2017).

As the spatial and temporal distribution of surface solar radiation depends on topographic effects and

shadows due to the horizon, spatial disaggregation methods have been demonstrated to be efficient to improve the spatial detail of existing, low resolution satellite datasets (Ruiz-Arias *et al.*, 2010). In particular, such methods are aimed at adding information related to the effects of topography, thus enhancing the accuracy of solar radiation estimates over irregular terrains. Following this research line, a procedure for predicting solar radiation over rugged terrains, named Estimation of global solar RADiation (ERAD), is currently put forward. This semi-empirical disaggregation method, which is similar to others proposed in the literature, performs a downscaling based on a DEM (Ruiz-Arias *et al.*, 2010; Haurant *et al.*, 2012; Moreno *et al.*, 2013). In particular, ERAD can improve the DSSF LSA SAF product, which has spatial and temporal resolutions of 5 km and 30 min, respectively, producing solar radiation estimates with a spatial resolution of 200 m and a time step of 1 min. The new disaggregation method is applied over a wide study area which includes Italy, and the estimates obtained are validated against a consistent dataset of daily ground observations taken from 2005 to 2016. An intercomparison is also performed versus radiation estimates obtained from three other standard methods, MTCLIM, LSA SAF and CAMS. Finally, the improvements produced by the new method over the other algorithms are highlighted by examining some examples of how the respective solar radiation estimates vary in space and time.

2 | RADIATION ESTIMATION METHODS

The next sections briefly introduce the three standard methods used for intercomparison, followed by a detailed description of the new ERAD algorithm.

2.1 | MTCLIM

MTCLIM is an indirect method for the simulation of daily solar radiation based on meteorological data usually collected in weather stations. The method uses the minimum and maximum daily temperature together with the daily precipitation and other geographical information such as latitude, elevation, slope and aspect (Thornton *et al.*, 2000). The application of MTCLIM over large regions with complex morphologies requires the preliminary extrapolation–interpolation of meteorological variables, such as those obtained by the DAYMET algorithm (https://daymet.ornl.gov) with 1 km resolution (Thornton *et al.*, 1997) or the European Observation database (https://www.ecad.eu), with 0.25° resolution (Haylock *et al.*, 2008). MTCLIM has a universal valence, being usable over a wide range of climates without reparameterization on a site-by-site basis.

Indeed, when applied to BSRN station data, the method produced reasonable results over most sites and under most geographical and climate conditions (Bohn *et al.*, 2013). The version of MTCLIM used in the present study is 4.3, although the empirical coefficients related to daily temperature range are those defined in the original version of the method (Thornton and Running, 1999).

2.2 | LSA SAF

The current MSG satellites are supported by EUMETSAT in collaboration with the European Space Agency. Additionally, EUMETSAT supervises and coordinates the activities of LSA SAF for routinely providing some solar radiation products, such as MSG DSSF (LSA-201), available at the website http://landsaf.ipma.pt. The DSSF products, obtained by the approach described by Geiger *et al.* (2008a), have the same projection and spatial resolution (3 km at nadir) as the original MSG imagery. Overall, DSSF mainly depends on the solar constant, the cosine of the solar zenith angle, the transmittance of the atmosphere (which is determined by cloud cover), the atmospheric absorption and scattering and the surface albedo. For the SAF products, the distribution of some atmospheric gases (water vapour and ozone) is derived from numerical weather forecasts of the European Centre for Medium-Range Weather Forecasts and the Total Ozone Mapping Spectrometer, respectively. The land surface albedo is derived from MSG, too (Geiger *et al.*, 2008a). In summary, the DSSF products are obtained by calculating the effective transmittance of the atmosphere, both in clear and cloudy sky conditions, and multiplying it for the solar constant. In the clear sky case, MSG data are not used and the transmittance is determined from a physical model of the atmosphere with visibility fixed to 20 km and a continental-type aerosol. Instead, in the cloudy sky case, a simple RTM is employed and the MSG observations are a fundamental input. In this case, in fact, more radiation is reflected by the clouds (brighter pixels in MSG images) and less radiation reaches the ground. However, some approximations are made, such as the one for which the whole image pixels are covered by a homogeneous cloud layer (Geiger *et al.*, 2008a). Therefore, the cloud transmittance of each pixel is related to cloud albedo by an empirical cloud absorption factor. The validation of the DSSF LSA SAF product yielded good results in different study regions (Journée and Bertrand, 2010; Cristóbal and Anderson,

2013). The DSSF product currently used (LSA-201) is disseminated every 30 min starting from 2005.

2.3 | CAMS

CAMS uses the Heliosat-4 method based on MSG imagery to produce solar radiation estimates, mostly at the site level, covering European and African regions since 2004. The Heliosat-4 method is a physical approach based on two libraries of RTMs that use look-up tables: the McClear and McCloud models (Qu *et al.*, 2017). One of the advantages of this method is that it allows the radiation received at ground level in all sky conditions to be estimated. The McClear model provides the clear sky irradiance, which is multiplied by a modification factor, while the McCloud model takes into account the effects of radiation extinction due to clouds. The main input variables (aerosol optical properties, water vapour and ozone) are updated every 3hr by CAMS on a global scale. Ground albedo is determined using Moderate Resolution Imaging Spectroradiometer (MODIS) imagery. The McCloud model uses the physical optical properties of the clouds (e.g. optical depth, type and coverage of cloud) derived from MSG observations, every 15 min and at 5 km of resolution, to calculate the cloudy sky irradiance. The Heliosat-4 model generally exhibits satisfactory performance (Marchand *et al.*, 2019) although some limitations are known (Qu *et al.*, 2017). The CAMS products are related to the solar radiation incoming on a horizontal surface of a certain site, for the actual weather conditions, at different time steps (from 1 min to 1 month). If not included in the user request, the CAMS service provides the altitude of the site on the basis of some DEMs available, including the Shuttle Radar Topography Mission data with 100 m of spatial resolution (CAMS, 2019). The current solar radiation product is downloaded through the website http://www.soda-pro.com.

2.4 | ERAD

ERAD is a semi-empirical method based upon a disaggregation procedure applied to the DSSF LSA SAF product and a DEM of the study area. This spatial disaggregation method consists in the redistribution of the estimated solar radiation evaluating carefully all topographic effects. The resolution of the used DEM must obviously be much higher than that of the original satellite data (5 km), so that the estimated solar radiation offers highly improved spatial detail over rugged terrains (Moreno *et al.*, 2013).

ERAD provides the solar radiation for each point of the DEM and 1 min time steps, similarly to the procedure of Haurant *et al.* (2012). As LSA SAF provides half-hourly solar radiation at a resolution of about 5 km, the disaggregation method concerns both spatial and temporal scales. The calculation of the daily solar radiation average integrates all estimates of the daytime, which requires some approximations. The most significant of these is the assumption of a homogeneous spatial distribution and a constant temporal variation of all variables considered in the radiation estimation process for each DEM point. A classical linear interpolation method is applied to the variables sampled at different time intervals compared to the basic 1 min step. The application of this method also requires the calculation of numerous astronomical features, such as the true and apparent solar position in the sky, or other geographical features such as the sky view factor (SVF), for each point of the DEM. All these features are defined on the basis of standard reference guidelines (e.g. Iqbal, 1983; Flint and Childs, 1987; Michalsky, 1988; Sengupta *et al.*, 2015). ERAD determines the solar radiation in two phases as described in the following sections.

2.4.1 | Half-hourly data processing

ERAD has as main input the half-hourly DSSF images provided by LSA SAF (LSA-201) product. An inversion of the physical model described by Geiger *et al.* (2008a) is applied to estimate the actual transmittance of the atmosphere by the clearness index (k_t) defined as the ratio (Skartveit *et al.*, 1998):

$$k_t = \frac{I_{gh}}{I_{0h}} \tag{1}$$

where I_{gh} and I_{0h} are the global and extraterrestrial global radiation, estimated on a horizontal surface.

In ERAD the extraterrestrial global radiation (I_{0h}) is calculated as (Iqbal, 1983):

$$I_{0h} = I_0 \left[1 + 0.033\cos\left(\frac{360 \cdot \mathrm{DOY}}{365}\right)\right]\cos(\theta_{SZA}) \tag{2}$$

where I_0 is the solar constant over the whole solar spectrum (1,367 $\mathrm{W \cdot m^{-2}}$) and the expression in square brackets corresponds to the Earth's orbit eccentricity factor, in which DOY is the day of the year. Instead, LSA SAF estimates k_t by integrating the radiation in a limited range of the solar spectrum, 300–4,000 nm, corresponding to a solar constant of 1,358 $\mathrm{W \cdot m^{-2}}$ (Geiger *et al.*, 2008a).

The cosine of apparent solar zenith angle (θ_{SZA}) can be expressed as a function of some astronomical parameters such as the DOY declination (δ), the latitude (Φ) and the hourly angle (ω) calculated at the centre point of each DEM pixel, in accordance with the acquisition times of the MSG overpasses:

$$\cos(\theta_{SZA}) = \sin(\delta)\sin(\Phi) + \cos(\delta)\cos(\Phi)\cos(\omega) \quad (3)$$

where Φ is known and δ and ω are calculated following Michalsky (1988).

The clearness index (k_t) is a dimensionless number between 0 and 1, and has a high value under clear sky and a low value under cloudy conditions. In some circumstances, such as in cloud enhancement situations or high albedo due to snowy conditions, k_t could exceed unity. A maximum threshold of k_t, equal to 0.9, is therefore imposed to avoid these situations. Moreover, k_t is calculated only when the solar zenith angle is less than 85° to avoid miscalculation problems when the sun is near the horizon.

At regional or local scale, the distribution of solar radiation is affected by elevation (z) which represents a topographic effect. In fact, due also to the reduction of the optical path length, an increase in altitude generally produces a rise of the global radiation incoming on the surface. The elevation correction is made for each point of the image considered. As the solar global radiation value $I_g(z_0)$ derived from the DSSF product is referred to sea level (z_0) (Moreno *et al.*, 2013), a z-correction is applied according to Wahab *et al.* (2010). Hence, given the global radiation at z_0, the global radiation at elevation z is obtained from the following empirical function:

$$I_g(z) = \frac{I_0}{\exp\left[\tau(z_0)\beta^{(z_0 - z)}\right]} \quad (4)$$

where $\tau(z_0) = -\ln[I_g(z_0)/I_0]$ and $\beta = 1.2$.

Consequently, for each elevation z of DEM point, a corrected clearness index k_t is defined as:

$$k_t(z) = \exp\left\{\ln[k_t(z_0)]\beta^{(z_0 - z)}\right\} \quad (5)$$

where $k_t(z_0) = I_g(z_0)/I_0$ and $z_0 = 0$. This obviously implies that every DEM point is associated with the nearest point on the k_t DSSF image. As the elevation effect on the global radiation is mainly due to the beam component of solar radiation, the elevation correction is applied only in prevailing clear sky conditions. These conditions are met when the correct clearness index k_t exceeds a threshold value of 0.65, in accordance with Ruiz-Arias *et al.* (2010).

After the elevation correction, ERAD uses a decomposition model to subdivide the global solar radiation received on a horizontal plane into beam and diffuse radiation components. Among the numerous decomposition models proposed in the literature (Bertrand *et al.*, 2015), the model of Skartveit *et al.* (1998) is used. This model is among the most widespread and has recently been found to be one of the most efficient in a comparison with 13 other models for a highly rugged area near Bolzano (northern Italy) (Laiti *et al.*, 2018). The model is based on three main input predictors: the solar zenith angle, the clearness index and a temporal variability index (hourly in the original model and semi-hourly in ERAD).

In this decomposition model, the clearness index depends also on the local land surface albedo, which is derived from the daily albedo product provided by LSA SAF dataset. Therefore, in the ERAD procedure, the Skartveit model allows the diffuse component of the solar radiation to be derived by the cloudiness index (k_d), defined as the ratio between diffuse (I_{dh}) and global (I_{gh}) solar radiation that reaches a horizontal surface:

$$k_d = \frac{I_{dh}}{I_{gh}} \quad (6)$$

The cloudiness index (k_d) is obtained with the same temporal resolution of DSSF product (30 min) and therefore k_d is assumed to remain constant in this time interval.

2.4.2 | One minute data processing

Since the position of the sun in the sky changes continuously throughout the day, the simulation of the other topographic effects on radiation distribution is performed using a 1 min time step. For this step, the global (I_{gh}), diffuse (I_{dh}) and beam (I_{bh}) solar radiation incoming on a horizontal surface are calculated for each DEM point on the basis of the previously determined parameters ($k_t(z)$, k_d) by means of the following equations:

$$I_{gh} = I_{0h} k_t(z) \quad (7)$$

$$I_{dh} = k_d I_{gh} \quad (8)$$

$$I_{bh} = I_{gh} - I_{dh} \quad (9)$$

Transposition models are then used to convert the solar radiation on the horizontal surface to that on the tilted surface (Padovan and Del Col, 2010) as determined by the DEM. These models define how the various components of solar radiation arrive on the terrain from the

sky and the surrounding land surface. SVF is a key factor to reach this objective since it takes into account the light conditions in relation to the DEM.

The first condition calculated for each time step (1 min) of the day is if the site (or point) considered is directly illuminated by the Sun or if it is in shade. Given the complexity of the actual lighting conditions, it is convenient to treat each of the solar radiation components separately and, lastly, sum the beam, diffuse and reflected components to obtain the daily global solar radiation incoming on the tilted surface.

The beam radiation component, on a tilted (T) surface (I_{bT}), follows a purely geometric relation with respect to the horizontal component (I_{bh}) (Iqbal, 1983). In fact, it depends on the following ratio:

$$r_b = \frac{\cos(\theta)}{\cos(\theta_{SZA})} \tag{10}$$

where θ is the incidence angle of the Sun's light rays compared to the normal at the tilted surface. $\cos(\theta)$ of Equation (10) can be obtained using the following expression:

$$\cos(\theta) = \cos(S)\cos(\theta_{SZA}) + \sin(S)\sin(\theta_{SZA})\cos(\psi - A) \tag{11}$$

where S and A are the slope and aspect, respectively, and ψ is the solar azimuth which can be derived from the formula:

$$\cos(\psi) = \sin(\delta)\sin(\phi) - \frac{\sin(\delta)}{\cos(\alpha)\cos(\phi)} \tag{12}$$

and α is the apparent solar elevation. Hence, the beam radiation component (I_{bT}) can finally be computed as:

$$I_{bT} = I_{bh} r_b s_b \tag{13}$$

The s_b factor in Equation (13), which will be described later, takes into account the Sun's position to determine the partial, or total, shading conditions for each DEM point.

For the sky diffuse radiation component the type of solar radiation distribution needs to be defined. For example, if an isotropic distribution model is assumed, the intensity of radiation is supposed to be uniform over the sky dome. The diffuse radiation incident on a tilted plane, with slope S, is usually approximated by multiplying the diffuse radiation on a horizontal surface (I_{dh}) by transposition factor or view factor to the sky of the diffuse component, which is given by $[1 + \cos(S)]/2$ (Demain *et al.*, 2013). ERAD instead uses the more accurate Hay anisotropic model, for which the diffuse radiation (I_{dh}) is divided into two components (Iqbal, 1983): an isotropic component (I_{di}), which implies a uniform radiation distribution from the sky, and a circumsolar anisotropic component (I_{dc}). The latter is related to the incoming radiation from the area surrounding the solar disc, which can be analysed as beam irradiation. As suggested from the Hay model, the two diffuse components are weighted according to an isotropy index, defined from the ratio I_{bh}/I_{0h}. Consequently, the isotropic radiation can be evaluated by $I_{di} = I_{dh}\,(1 - I_{bh}/I_{0h})$ while the circumsolar radiation is evaluated by $I_{dc} = I_{dh}\,I_{bh}/I_{0h}$. Moreover, the diffuse radiation received by a tilted surface also depends on some topographic factors. In fact, taking into account the SVF for each point of the DEM, the isotropic diffuse radiation will be limited by the horizon, and therefore from the SVF value ($0 < \text{SVF} < 1$), except in the case of a wide flat area for which SVF = 1. Hence, similarly to Aguilar *et al.* (2010), given the diffuse solar radiation on a horizontal surface (I_{dh}), the diffuse and circumsolar radiation components on a tilted surface, I_{diT} and I_{dcT} respectively, are obtained from the following equations:

$$I_{diT} = I_{dh}\left(1 - \frac{I_{bh}}{I_{0h}}\right)\text{SVF} \tag{14}$$

$$I_{dcT} = I_{dh}\frac{I_{bh}}{I_{0h}} r_b s_{dc} \tag{15}$$

where SVF is a function of slope (S), aspect (A) and local horizon angle ($\alpha_{hor,i}$), in each of N_d directions i, equally distributed on the plane selected starting from the centre of each DEM point. More specifically, SVF is obtained by integrating in all directions i, with azimuth $i(360/N_d)$, the following expression, equivalent to that suggested by Dozier and Frew (1990):

$$\text{SVF} = \left(\frac{1}{N_d}\right)\sum_i \{\cos(S)[\cos(\alpha_{hor,i})]^2 + \sin(S)\cos(\gamma_i) \left[\left(\tfrac{\pi}{2} - \alpha_{hor,i}\right) - \sin(\alpha_{hor,i})\cos(\alpha_{hor,i})\right]\} \tag{16}$$

where N_d is the number of directions i (72 in the present study), the summation is evaluated for each direction i, and γ is the difference between the azimuth of each direction i and the aspect (A) of the surface considered.

The s_b and s_{dc} factors in Equations (13) and (15) define the shadowing conditions for the beam and diffuse-circumsolar components, respectively. In fact, the shading from the Sun depends on the Sun's position referred to the horizon. This phenomenon is usually taken into account by a discrete Heaviside step

function, whose values are 0, 0.5 or 1 when the Sun is below, halfway or above the horizon, respectively (Ruiz-Arias *et al.*, 2010). A similar function is currently used for the s_b and s_{dc} factors, which differ from the classical Heaviside function when the Sun is partially obscured from the horizon. In this case the value of s_b, or s_{dc}, is not 0.5 but is variable between 0 and 1, equal to the ratio between the area of the solar segment which is visible and the total area of the solar disc. The circumsolar radiation instead corresponds to a region around the solar disc (solar aureole). In accordance with the measurements of Flint and Childs (1987), the circumsolar region, viewed from each DEM point, is defined by a cone of sunlight with an opening angle of 4°; the same cone, relative to the solar disc alone, is on average 0.52°.

The last component of global solar radiation incoming on a tilted surface is the ground-reflected radiation. As ground albedo and topography can vary also over a short distance, their interaction can lead to a high variability of the radiation field, in terms of both intensity and spatial–temporal distribution. Since the surface reflection characteristics are not easy to find, the reflected radiation component is usually assumed to be isotropic. In this case, each surface point reflects a constant radiance, as a perfectly diffuse reflector, which depends on the view factor to ground: $(1 - \cos(S))/2$ (Demain *et al.*, 2013). In the present study, knowing the global solar radiation on a horizontal surface (I_{gh}), the reflected radiation on a tilted surface (I_{rT}) coming from the surrounding terrain is estimated using the following equation (Aguilar *et al.*, 2010):

$$I_{rT} = I_{gh}\rho\left[\frac{1+\cos(S)}{2} - \mathrm{SVF}\right] \tag{17}$$

where ρ is the regional albedo derived from the LSA SAF dataset. The term in square brackets in Equation (17) represents the terrain transposition factor, or view factor to the ground of the reflected component, named ground view factor (GVF). In the case of a horizontal surface ($S = 0$), the GVF is complementary to SVF, so that GVF = 1 − SVF. The estimation of the ground albedo is fundamental for the assessment of reflected radiation, but the assumptions of isotropy for this radiation and of daily constant distribution for ρ are both unrealistic. In particular, ρ shows a high rate of daily and seasonal variability due to various factors, such as changes in soil water content, vegetation status, snow cover (Demain *et al.*, 2013).

The global solar radiation on a tilted surface corrected for all topographic effects (I_{gT}) is therefore obtained for each minute as the sum of all solar components derived from Equations (13)–(17):

$$I_{gT} = I_{bT} + I_{dcT} + I_{diT} + I_{rT} \tag{18}$$

The global solar radiation on a horizontal surface is obviously obtained using $S = 0$ in each of the above defined components. In the case of daily outputs, the

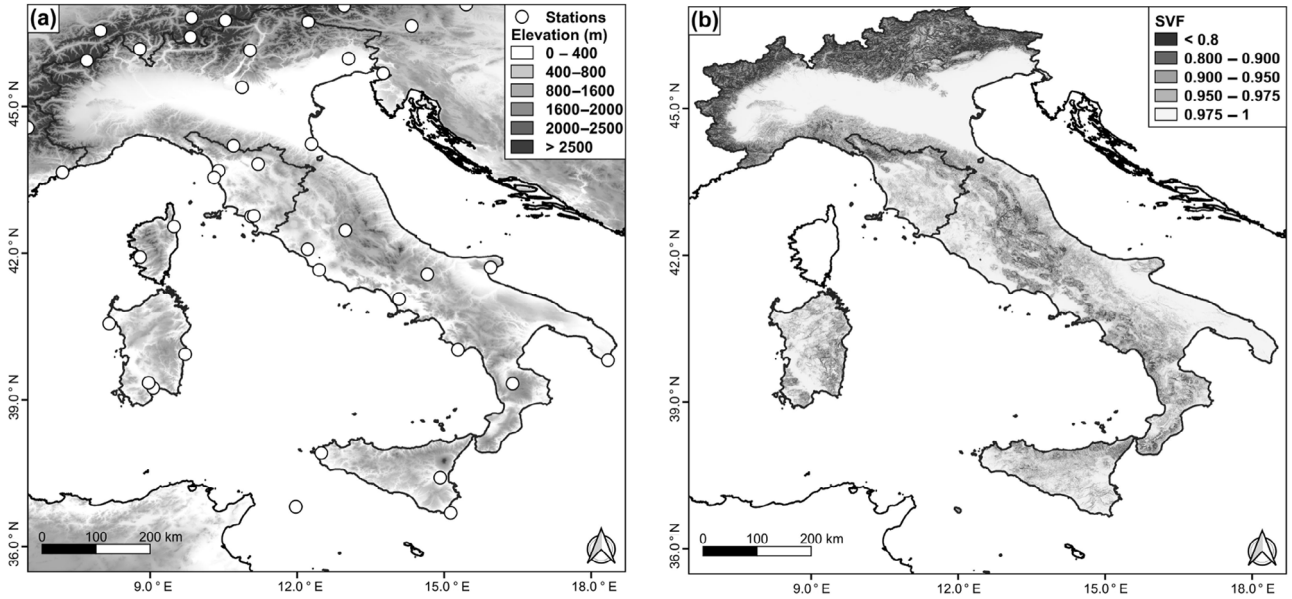

FIGURE 1 Elevation (a) and sky view factor (SVF) (b) maps derived from a digital elevation model with 200 m cell size; the white circles in (a) indicate the 43 weather stations currently considered

TABLE 1 Name, elevation, geographical coordinates and time range of the 43 weather stations used

Elevation class, station name	Elevation (m)	Latitude (° N)	Longitude (° E)	Start_time (YYYYMMDD)	End_time (YYYYMMDD)
Plain	< 200				
Trieste	2	45.6769	13.7547	20050103	20161231
Pisa	2	43.6825	10.3956	20110902	20150701
Grosseto	3	42.7481	11.0589	20110902	20130406
Trapani Birgi	3	37.9142	12.4914	20050103	20160401
Nice	4	43.6489	7.2089	20050103	20160401
Grazzanise	5	41.0606	14.0789	20050122	20151014
Cagliari Elmas	5	39.2436	9.0600	20050103	20130617
Cervia	6	44.2289	12.2919	20110906	20150701
Ajaccio	9	41.9181	8.7928	20050103	20160401
Bastia	12	42.5406	9.4853	20050103	20160401
Grosseto_(LAMMA)	20	42.7606	11.1152	20130115	20161231
Decimomannu	21	39.3461	8.9675	20110902	20130501
Pratica di Mare	23	41.6556	12.4481	20110902	20150701
Catania Sigonella	23	37.4056	14.9186	20110902	20150507
Livorno_(LAMMA)	30	43.5471	10.3046	20150213	20161231
Sesto_Fiorentino_(LAMMA)	57	43.8189	11.2021	20050201	20161231
Cozzo Spadaro	43	36.6861	15.1314	20110902	20150501
Udine Rivolto	54	45.9756	13.0492	20050103	20100410
Verona Villafranca	65	45.3881	10.8733	20050303	20120501
S. Maria di Leuca	112	39.8115	18.3423	20110129	20150701
Capo Bellavista	138	39.9308	9.7131	20051120	20111101
Capo Palinuro	160	40.0250	15.2803	20070717	20150701
Pantelleria	190	36.8139	11.9711	20050202	20090301
Hill	200–800				
Capo Caccia	204	40.5611	8.1631	20110902	20130201
Vigna di Valle	270	42.0801	12.2114	20050105	20161231
Graz Universitat	366	47.0778	15.4489	20050103	20160401
Locarno Monti	375	46.1725	8.7875	20050103	20160401
Klagenfurt-Flughafen	447	46.6428	14.3372	20050103	20160401
Payerne	491	46.8150	6.9440	20050103	20160401
Campobasso	786	41.5636	14.6550	20110911	20150701
Mountain	> 800				
Monte Sant'Angelo	844	41.7083	15.9478	20110903	20150701
Embrun	871	44.5656	6.5022	20050103	20160401
Dobbiaco	1,226	46.7267	12.2243	20050602	20161231
San Valentino alla Muta	1,461	46.7619	10.5344	20110908	20150701
Davos	1,610	46.8131	9.8436	20050103	20160401
Monte Scuro	1,720	39.3297	16.3957	20050103	20151231
Monte Terminillo	1,752	42.4667	12.9833	20050103	20090901
Paganella	2,129	46.1434	11.0375	20110902	20150701
Monte Cimone	2,173	44.1937	10.7003	20110902	20150701
Sonnblick	3,109	47.0540	12.9570	20050103	20160401
Piz Corvatsch	3,315	46.4181	9.8211	20050103	20160401
Jungfraujoch	3,471	46.5469	7.9836	20050103	20160401
Plateau Rosà	3,488	45.9354	7.7073	20110902	20120701

global solar radiation is obtained by integrating Equation (18) over all 1,440 min of a day.

3 | ASSESSMENT OF THE METHODS

3.1 | Study area and data

The four radiation estimation methods were assessed in an area which corresponds to the land surface of Italy and its surroundings (Figure 1a,b). This area is characterized by a wide variety of morphological, vegetation cover and climatic features. Due to the presence of the Alps chain in the north and the Apennines chain along the ridge of the peninsula, the Italian landscape is prevailingly mountainous and hilly. Most of the country benefits from a typical Mediterranean climate characterized by warm dry summers and mild wet winters.

Figure 1a shows the DEM of the study area with the position of the 43 weather stations currently used. The DEM lies between 35.05 ° and 47.18 ° N and 6.50 ° and 19.71 ° E and is derived from Shuttle Radar Topography Mission data (SRTM-3, http://srtm.csi.cgiar.org) after a resampling to 7.5 arc second (about 200 m in the study area) from the original resolution of 3 arc second. The DEM area extends outside the Italian State and includes various weather stations in the surrounding countries. In addition to elevation, other morphological parameters such as slope (S) and aspect (A) are directly derived from the DEM by standard algorithms. The DEM is also used for calculation of the SVF, which is defined as the fraction of sky visible above a certain ground observation point (Dozier and Frew, 1990) (Figure 1b).

Table 1 indicates the elevations, the geographical coordinates and the periods of data collection of the weather stations used in the study. The stations are ordered with increasing elevation and are divided into three categories (plain, hill and mountain) if their altitude is less than 200, between 200 and 800 and higher than 800 m above sea level, respectively. Apart from some stations of the LaMMA Consortium, Sesto Fiorentino, Livorno and Grosseto, most of these stations belong to the WRDC-WMO network; two exceptions are Payerne and Sonnblick, which belong to the BSRN.

3.2 | Performance evaluation

The performances of the estimation methods considered (MTCLIM, LSA SAF, CAMS and ERAD) were evaluated both quantitatively and qualitatively. The first assessment was carried out versus daily global solar radiation observations taken at the 43 reference ground stations over the period 2005–2016. Since all these observations are referred to horizontal surfaces, their use for the current purpose had to rely on some assumptions which are discussed in Section 5.

The four methods used different drivers (input data). Both MTCLIM and ERAD used the available DEM. Additionally, MTCLIM required daily temperature and rainfall measurements, while the other methods used half-hourly MSG imagery. Each estimated data series therefore showed a different number of missing values, which were due to various causes (data processing system failures, the application of filtering criteria, etc.). For example, the average daily global solar radiation could not be computed when some diurnal cycles of the MSG images were missing and therefore not representative of all daytime. The data series estimated by MTCLIM, LSA SAF, CAMS and ERAD for all ground stations consisted of 94,635, 59,240, 94,393 and 95,069 daily samples, respectively. The MTCLIM, CAMS and ERAD datasets had about 48% missing data in the period examined, while LSA SAF dataset had about 37% additional missing data. Finally, the common dataset of measured and estimated daily solar radiation data consisted of 57,534 daily samples, which were used for the accuracy assessment.

The accuracy of each method was summarized by means of common statistics, that is, the mean bias error (MBE), the mean absolute error (MAE) and the root mean square error (RMSE), computed using the following equations:

$$\mathrm{MBE} = \frac{1}{N}\sum_i (e_i - o_i) \tag{19}$$

$$\mathrm{MAE} = \frac{1}{N}\sum_i |e_i - o_i| \tag{20}$$

$$\mathrm{RMSE} = \sqrt{\left[\frac{1}{N}\sum_i (e_i - o_i)^2\right]} \tag{21}$$

where e_i and o_i are the estimated and observed daily values, respectively, for every day sampled (i) on all data series (N) considered. To obtain dimensionless errors, these statistics were also transformed into percentages (%), dividing each value by the average of the ground observations and multiplying by 100. The accuracy assessment was completed by calculating the coefficient of determination (R^2) between measurements and estimates. All these statistics were computed both considering all ground stations and these aggregated by elevation (plain, hill and mountain).

The performances of the radiation methods considered were also qualitatively evaluated by visually

analysing the spatial and temporal variations of the respective solar radiation estimates. In the case of MTCLIM, high spatial resolution daily radiation maps could be obtained only for a region of Italy, Tuscany, where the DAYMET interpolation algorithm had been applied to a great number of ground meteorological observations and the same DEM used in the present study. For LSA SAF the visual analysis was obviously limited only to the comparison between the estimates of solar radiation on a horizontal surface; the average annual map was produced by integrating all available daily data for which no SAF product (semi-hourly) during the diurnal cycle was missing. CAMS limits the number of daily requests and prevents the acquisition of solar radiation estimates at area level. Actually, CAMS provides also a gridded product, whose spatial resolution (0.2°), however, is incompatible with that of the DEM currently used. Thus, only ERAD could be applied to the entire Italian territory to produce high spatial resolution (200 m) solar radiation estimates over rugged terrains taking into account all topographic effects; this exercise was carried out for an exemplary year (2015), yielding 30 min images which were finally aggregated to an annual map.

TABLE 2 Number of common observations in the considered datasets (*N*) and mean annual global solar radiation observed (Mean) for all stations (All) and for stations grouped by elevation (Plain, Hill and Mountain)

	N	Mean ($W \cdot m^{-2}$)
All	57,534	169.3
Plain	27,233	176.7
Hill	12,354	154.5
Mountain	17,947	168.2

4 | RESULTS

4.1 | Quantitative evaluation of estimated radiation

All 43 ground stations currently considered are placed in areas where solar radiation is not affected by the surroundings reliefs; for all stations, in fact, the SVF is greater than 0.94. Tables 2 and 3 summarize the results of the statistical evaluation of the solar radiation estimates obtained by the four models at these stations. More particularly, Table 2 shows the numbers of observations and the daily global solar radiation averages of the measured data series for all stations and for these aggregated

TABLE 3 Accuracy statistics (all errors are in $W \cdot m^{-2}$ and (%)) obtained for MTCLIM, LSA SAF, CAMS and ERAD considering all 43 stations (row All) or stations aggregated by elevation (rows: Plain, Hill, Mountain)

	MTCLIM	LSA SAF	CAMS	ERAD
MAE				
All	35.1 (20.7)	16.8 (9.9)	19.3 (11.4)	16.7 (9.9)
Plain	32.9 (18.6)	11.6 (6.6)	13.4 (7.6)	12.9 (7.3)
Hill	30.4 (19.7)	11.5 (7.5)	14.6 (9.5)	12.4 (8.0)
Mountain	41.7 (24.8)	28.3 (16.8)	31.5 (18.7)	25.4 (15.1)
RMSE				
All	48.4 (28.6)	25.4 (15.0)	30.0 (17.7)	25.3 (14.9)
Plain	44.4 (25.2)	17.6 (10.0)	19.9 (11.3)	19.2 (10.9)
Hill	41.9 (27.1)	15.5 (10.1)	20.5 (13.3)	16.9 (10.9)
Mountain	57.4 (34.2)	37.9 (22.5)	44.7 (26.6)	36.0 (21.4)
R^2				
All	0.768	0.940	0.911	0.943
Plain	0.899	0.973	0.961	0.972
Hill	0.825	0.977	0.959	0.975
Mountain	0.670	0.884	0.812	0.882
MBE				
All	−4.4 (−2.6)	−5.1 (−3.0)	−0.2 (−0.1)	2.0 (1.2)
Plain	−7.8 (−4.4)	2.1 (1.2)	1.6 (0.9)	6.7 (3.8)
Hill	−0.2 (−0.2)	−2.9 (−1.9)	2.9 (1.9)	2.9 (1.9)
Mountain	−2 0 (−1.2)	−17.5 (−10.4)	−4.9 (−2.9)	−5.7 (−3.4)

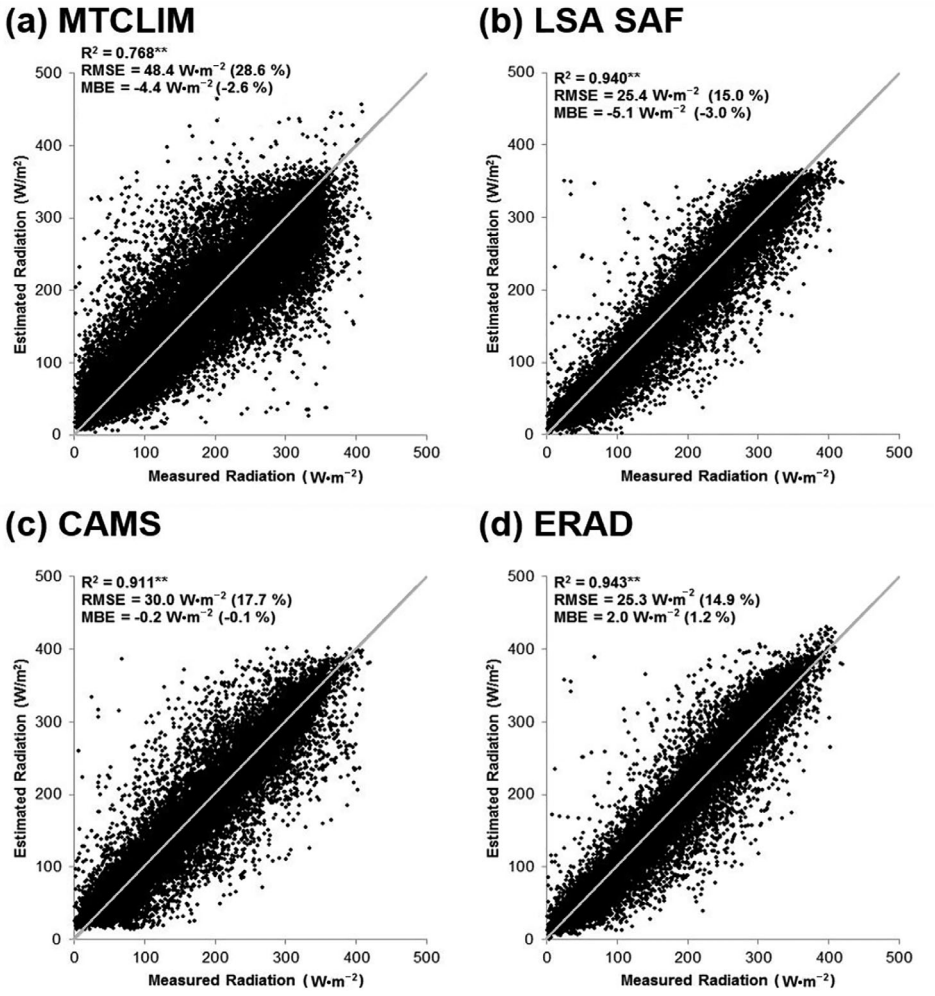

FIGURE 2 Scatterplots between daily global solar radiation measured and estimated by the four models for all stations (**highly significant correlation, $p < 0.01$)

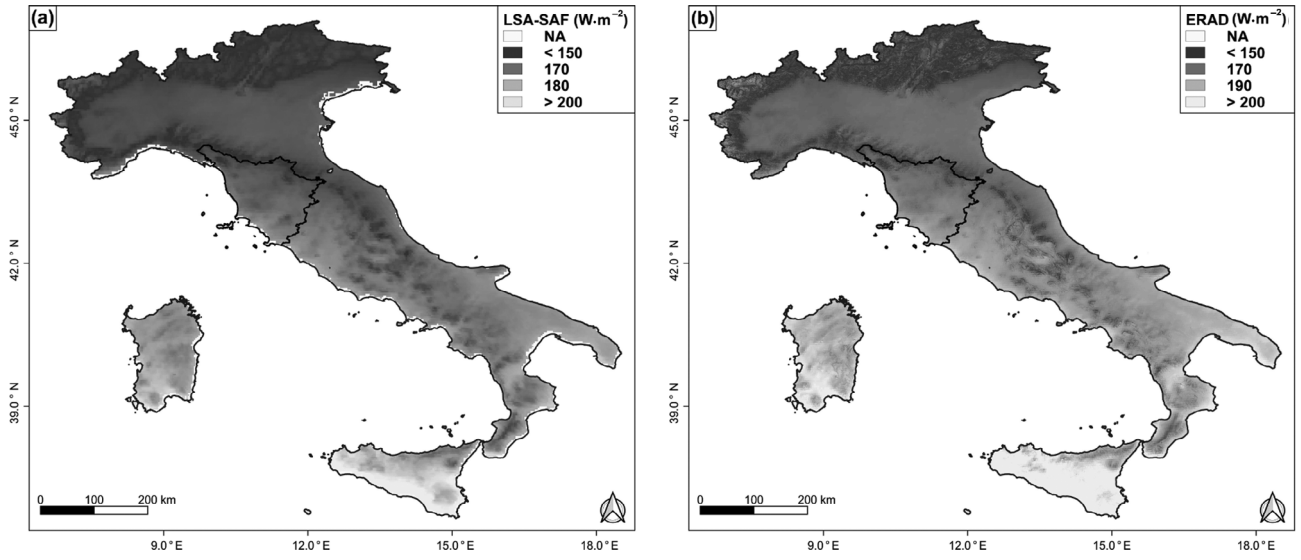

FIGURE 3 Mean annual daily global solar radiation, estimated on a horizontal surface, by LSA-SAF (a) and ERAD (b) for the Italian territory in 2015

by elevation (plain, hill and mountain), while Table 3 shows the accuracy statistics obtained by each method referred to both the original and percentage values.

Overall, MTCLIM provides the worst performance in terms of MAE, RMSE and R^2 (35.1 W·m^{-2}, 20.7%; 48.4 W·m^{-2}, 28.6%; and 0.768) followed by CAMS, LSA SAF and ERAD. The last two models show similar results, but ERAD is slightly more accurate (16.7 W·m^{-2}, 9.9%; 25.3 W·m^{-2}, 14.9%; and 0.943). The averaged MBEs of MTCLIM, LSA SAF and CAMS are moderately or marginally negative (underestimation) (–4.4 W·m^{-2}, –2.6%; –5.1 W·m^{-2}, –3.0%; and –0.2 W·m^{-2}, –0.1%; respectively) while ERAD presents a marginal overestimation (2.0 W·m^{-2}, 1.2%).

These results are confirmed by Figure 2, which displays the scatterplots of daily global solar radiation measured and estimated by the four models for all stations. The estimates of MTCLIM show the greatest dispersion around the 1:1 line, which testifies to the worst performance of this model. The results are better for LSA SAF and CAMS, but the former model shows a clear underestimation for the highest radiation values. Overall, ERAD has the smallest dispersion and no clear over/underestimation pattern.

The results are slightly different when considering the observations divided into the three elevation ranges (Table 3); the interpretation of these results, however, is complicated by the incomplete concordance of the four accuracy statistics, particularly the MBE.

As regards plain stations, MTCLIM, LSA SAF, CAMS and ERAD yield the following MBEs: −7.8 W·m^{-2} (−4.4%), 2.1 W·m^{-2} (1.2%), 1.6 W·m^{-2} (0.9%) and 6.7 W·m^{-2} (3.8%), respectively. MTCLIM therefore shows a strong underestimation of solar radiation, which is in contrast with the overestimation of the other models. Similar MBEs are found for hill stations. MTCLIM and LSA SAF present a slight underestimation, −0.2 W·m^{-2} (−0.2%) and −2.9 W·m^{-2} (−1.9%), while CAMS and ERAD show a slight overestimation, both equal to 2.9 W·m^{-2} (1.9%).

All models show the poorest accuracies over mountains, accompanied by a tendency to underestimate solar radiation; the negative MBE is marginal for MTCLIM, −2.0 W·m^{-2} (−1.2%), and maximum for LSA SAF, −17.5 W·m^{-2} (−10.4%). For CAMS and ERAD the MBEs are −4.9 W·m^{-2} (−2.9%) and −5.7 W·m^{-2} (−3.4%), respectively.

4.2 | Qualitative evaluation of estimated radiation

As previously mentioned, the qualitative assessment of the solar radiation products concerned the Italian territory for the year 2015. Figure 3a,b shows the maps of mean annual daily global solar radiation estimated by LSA SAF (a) and ERAD (b), respectively, on a horizontal

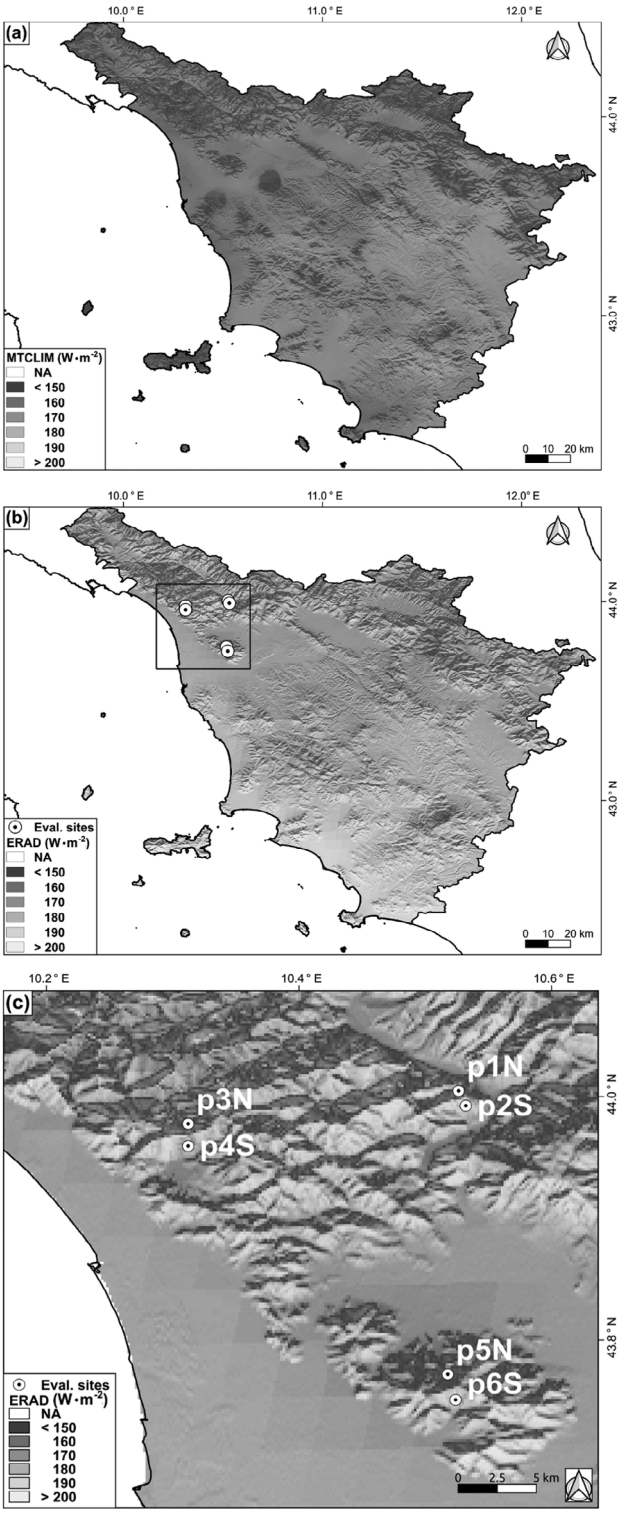

FIGURE 4 Mean annual daily global solar radiation, estimated for 2015, by MTCLIM (a) and ERAD (b) in a region of complex topography (Tuscany). The positions of three pairs of evaluation sites having opposite north–south aspects are shown in (b), (c)

TABLE 4 Morphological features of the evaluation sites shown in Figure 4c and global solar radiation averages estimated by the four models for 2015

Evaluation sites	Ele. (m)	Slo. (°)	Asp. (° N)	SVF	MTCLIM ($W \cdot m^{-2}$)	LSA SAF ($W \cdot m^{-2}$)	CAMS ($W \cdot m^{-2}$)	ERAD ($W \cdot m^{-2}$)
p1N	341	18	13	0.94	137	163	176	134
p2S	333	18	193	0.92	164	163	176	174
p3N	**539**	**30**	**7**	**0.87**	**115**	**162**	**177**	**105**
p4S	**518**	**33**	**199**	**0.90**	**160**	**162**	**176**	**173**
p5N	454	25	352	0.93	125	160	177	118
p6S	482	30	185	0.91	162	164	179	180

Abbreviations: Asp., aspect; Ele., elevation; Slo., slope; SVF, sky view factor, dimensionless.

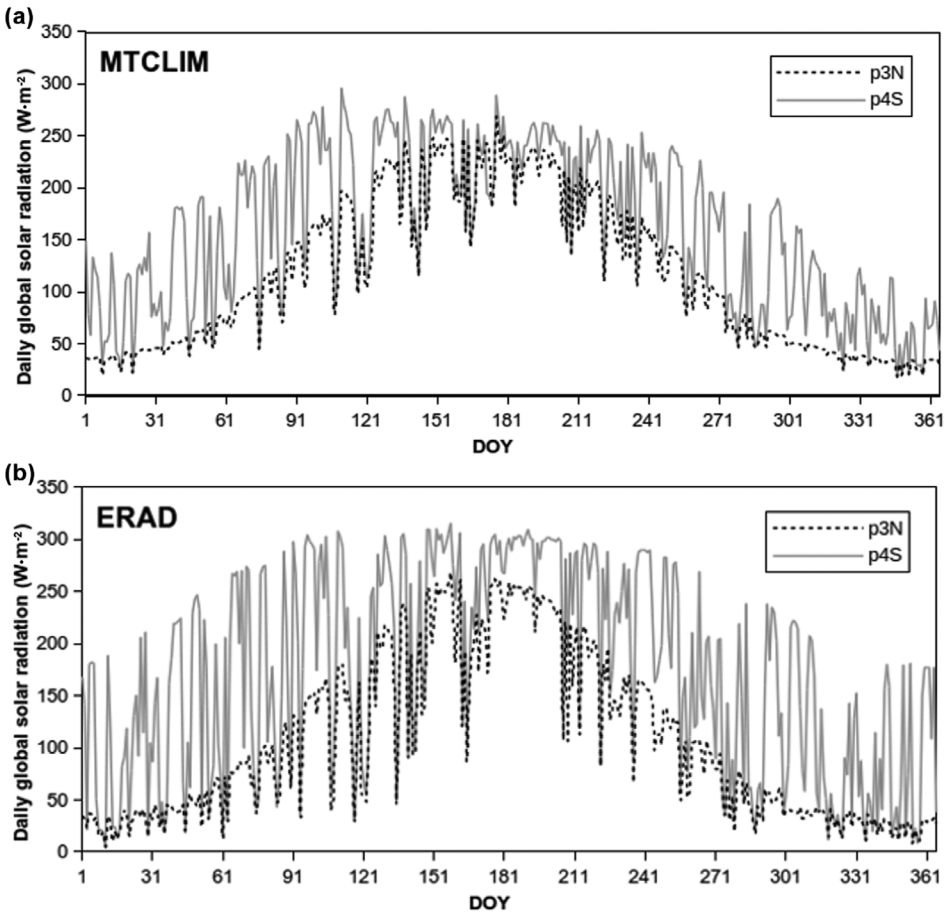

FIGURE 5 Annual trends of daily global solar radiation estimated by MTCLIM (a) and ERAD (b) for the second site pair of Figure 4c and Table 4 (p3N–p4S) in 2015

surface. The estimates of the two methods have a similar spatial distribution, but the former model predicts lower radiation values particularly over mountain areas.

Figure 4a,b shows the maps of mean annual daily global solar radiation estimated by MTCLIM (a) and ERAD (b), respectively, in a region of complex topography (Tuscany). MTCLIM produces generally reasonable radiation estimates, but with some anomalies which are probably associated with areas having a low density of the meteorological station network in 2015. This defect is not visible in the map obtained by ERAD, which simulates solar radiation as expected considering all described topographic effects.

Both Figures 3a,b and 4a,b confirm the expected trends of solar radiation related to latitude and elevation. There is an increase of mean solar radiation for lower latitudes due to different solar elevation angles and a decrease of radiation for mountain areas due to increased cloudiness and, in narrow and deep valleys, to the shading by mountain slopes.

The performances of MTCLIM and ERAD are further analysed by examining the annual radiation evolutions estimated for three pairs of sites situated over north–south slopes in a Tuscany mountain area (Figure 4b,c). Table 4 shows the main morphological features of these sites and the daily global solar radiation averages estimated by the four models for 2015.

LSA SAF and CAMS are both incapable of differentiating the solar radiation incident on different slopes. In contrast, both MTCLIM and ERAD can reasonably reproduce the higher solar radiation expected for southern slopes. The latter model, however, predicts higher radiation differences between contrasting slopes, that is, a higher effect of topography.

Figure 5a,b more clearly illustrates the annual trends predicted by the last two models for the second site pair. Both models simulate a prevalence of direct radiation incoming on the southern slope, with consequently higher day-to-day variability with respect to the northern slope, where diffuse radiation prevails. In accordance with what is observed above, these features are more pronounced for ERAD, that is, this model shows a higher sensitivity to the contrasting topographic characteristics of the two sites (Figure 5b).

5 | DISCUSSION

The current study has put forward a new method to predict global solar radiation over rugged terrains, ERAD. The method performs a disaggregation of LSA SAF data using a DEM with a spatial resolution of 200 m. Being based on LSA SAF data, ERAD presents most of the approximations brought by this product but provides more spatially and temporally detailed radiation estimates related to the resolution of the DEM used and the time step applied for data processing.

The results of ERAD have been inter-compared with those of three other standard models (MTCLIM, LSA SAF and CAMS) using daily solar global radiation observations taken in 43 stations in or around the Italian peninsula during the years 2005–2016. As is the case for almost all other solar radiation measurements taken worldwide, these observations are not optimal for the current purpose, being referred to horizontal surfaces. The model validation had therefore to rely on the assumption that an accurate estimation of the main radiation components (direct and diffuse) in this situation is a fundamental pre-requisite for a similar prediction over tilted surfaces (Ruiz-Arias *et al*., 2011). According to the theory presented in Section 2.4.1, the estimation of these components is intrinsically associated with that of global solar radiation, which has actually been assessed versus ground observations. The validity of this indirect evaluation strategy, which has been used by other authors (see for example Moreno *et al*., 2013), is obviously dependent on the soundness of the physical theory applied for redistributing the estimated radiation components in all sky–terrain conditions. Particular attention was therefore devoted to using a straightforward theoretical background capable of taking into account the impact of numerous interacting astronomical, geographical, topographic and atmospheric factors on radiation simulation.

Based on these premises, the performances of ERAD and the other models have been quantitatively analysed by the use of standard accuracy statistics. Overall, the improvement produced by ERAD is particularly evident with respect to MTCLIM and marginal with respect to LSA SAF and CAMS. Considering all 43 ground stations, ERAD yields the best accuracy, with a MAE of 16.7 $W{\cdot}m^{-2}$ (9.9%), RMSE of 25.3 $W{\cdot}m^{-2}$ (14.9%), R^2 of 0.943 and MBE of 2.0 $W{\cdot}m^{-2}$ (1.2%).

This analysis was completed by an assessment in three altitude belts, which indicates some peculiarities in the performance of the four methods. MTCLIM shows a clear radiation underestimation in plain areas, which probably derives from the presence of some coastal sites where the MBEs are strongly negative. For example, considering only the coastal stations of Pantelleria, Livorno and Nice, the MBEs are −35.2, −34.3 and −29.7 $W{\cdot}m^{-2}$ respectively. As noted by Bohn *et al*. (2013), these patterns probably depend on the low daily temperature ranges usually found in coastal areas, which affect MTCLIM simulation of diffuse radiation.

LSA SAF shows a general tendency to underestimate solar radiation, which is most evident over mountains, while ERAD shows a marginal overestimation over plains and hills, which is reversed at higher altitudes. These differences can be attributed to the use of slightly different radiation constants by LSA SAF and ERAD (1,358 and 1,367 $W{\cdot}m^{-2}$, respectively) and to ERAD accounting for the dependence of atmospheric transmittance on altitude, which is neglected by LSA SAF. The latter factor is obviously most influential over mountains, and this explains the almost complete correction of the radiation underestimation caused by LSA SAF in these cases. These results are similar to those obtained by Moreno *et al*. (2013) in a study conducted over Peninsular Spain; also these authors, in fact, found a clear radiation underestimation brought by LSA SAF in mountain areas, which was fixed by the application of an elevation correction.

Next, a qualitative evaluation was carried out using exemplary annual series of solar radiation maps produced by three of the models (MTCLIM, LSA SAF and ERAD). This analysis confirms the expected latitude and

altitude trends of the solar radiation estimates, which originate from the astronomical and topographic factors mentioned previously. The same analysis confirms that ERAD, as well as MTCLIM, can take into account the effect of surface tilting, which is not considered by LSA SAF and CAMS. The performances of MTCLIM and ERAD over rugged terrains have therefore been analysed by examining the radiation evolution on some site pairs having contrasting north–south aspects. Such analysis shows that ERAD is more sensitive than MTCLIM to topographic effects, that is, more clearly differentiates the solar radiation incoming on slopes with different aspects. In particular, the greater differentiation of north and south slopes predicted by ERAD is due to higher fractions of direct radiation estimated on clear days, which also leads to greater radiation drops on cloudy days and, consequently, to higher day-to-day radiation variability.

While a direct assessment of these different radiation trends is prevented by the mentioned lack of measurements on tilted surfaces, it can be noted that the limits of MTCLIM are widely recognized in the literature and have been confirmed by the current quantitative analyses. These limits are mostly related to the operational nature of this method, which uses standard daily meteorological observations (i.e. temperature range and rainfall) to model atmospheric conditions and consequently estimate direct and diffuse radiation fractions. These considerations lead reasonably to presume a higher accuracy of the radiation evolution predicted by ERAD over rugged terrains.

Such expected better performance is also related to the use of a 1 min time step to calculate all model variables, which corresponds to a temporal frequency much higher than that of the original LSA SAF product (half an hour). This choice should particularly affect the characterization of some topographic factors, such as the SVF, theoretically leading to a higher accuracy of the solar radiation estimates. The actual impact of this choice on the radiation estimation accuracy, however, has not been currently ascertained and could be the subject of future investigations.

In general, our analyses have confirmed the critical importance of the main DEM characteristics for disaggregating solar radiation over rugged terrains. It must in fact be recalled that the proper definition of surface slopes and aspects is dependent on the spatial resolution and accuracy of the DEM used (Kang-tsung and Bor-wen, 1991). The current choice of a medium resolution DEM (200 m) is dictated by both theoretical constraints and operational reasons. The low spatial resolution of the original satellite product (5 km), in fact, poses limits to the prediction of atmospheric variability in much smaller areas (CAMS, 2019). At the same time, the resolution chosen allows the straightforward production of daily radiation image series over the study area for a relatively long time period.

The improvements brought by ERAD do not concern other limits of the LSA SAF product, such as the assumption of isotropic and constant albedo within each 5 km pixel. The approximations brought by such an assumption should be of minor importance in most situations, and the same is true for the improvements brought by the possible use of higher spatial resolution albedo estimates, such as those produced by the MODIS system (Carrer *et al*., 2010).

Finally, in the near future, ERAD will be able to use, in place of the current DSSF LSA-201 product, the new DSSF LSA-207 product, which became operational from April 3, 2020. The latter product, available every 15 min, shows some important improvements particularly concerning the definition of the aerosol scheme used in a cloudless atmosphere (Ceamanos *et al*., 2014a; 2014b; Carrer *et al*., 2019a; 2019b). Moreover, this new product directly provides the diffuse component of solar radiation derived from a standard decomposition model (Reindl *et al*., 1990). These characteristics are expected to improve the accuracy of LSA SAF data and, consequently, that of ERAD estimates.

6 | CONCLUSIONS

The quantification of solar radiation is crucial to characterize the global phenomena related to climate and climate change (Wild, 2016). At a more local level, the prediction of the solar radiation incoming on complex morphologies is decisive to improve evapotranspiration estimates (Aguilar *et al*., 2010), to predict crop and forest yield (Chirici *et al*., 2016) and to plan the generation of electric power by photovoltaic systems (Demain *et al*., 2013).

The new method currently proposed to predict solar radiation over rugged terrains, ERAD, disaggregates the LSA SAF product by modelling the distribution of solar radiation over a digital elevation model having a spatial resolution of 200 m. The theoretical bases of ERAD have been thoroughly presented, followed by a testing of the model in comparison with other three standard methods (MTCLIM, LSA SAF and CAMS).

The results of this intercomparison indicate that, over horizontal surfaces, the solar radiation estimates produced by ERAD are notably more accurate that those of the other algorithm specifically conceived for operational application on rugged terrains, MTCLIM. The radiation estimates produced by ERAD have an accuracy similar to those of LSA SAF and CAMS, but higher spatial and

temporal resolutions (200 m and 1 min). Consequently it can be presumed that also over tilted surfaces the new model is capable of providing solar radiation estimates having enhanced details in space and time. This quantitative assessment has been completed by a qualitative evaluation of the variability of the radiation estimates produced by the four methods, which supports the same conclusion.

ERAD is therefore reasonably efficient in reproducing the spatio-temporal variations of solar radiation over rugged areas. In particular, this method is suitable for achieving the main practical objective of the current investigation, which is the completion of an existing database containing medium-term series of temperature and rainfall observations for the entire Italian national territory (Maselli *et al.*, 2012; Fibbi *et al.*, 2016).

ACKNOWLEDGEMENTS

The authors want to thank EUMETSAT and CAMS for providing the solar radiation products and WRDC-WMO, WRMC-BSRN and LaMMA Consortium for providing the solar radiation data measured in the weather stations. Finally, the authors thank the two anonymous reviewers for their insightful comments on the original manuscript.

ORCID

Luca Fibbi https://orcid.org/0000-0001-6985-6809

REFERENCES

Aguilar, C., Herrero, J. and Polo, M.J. (2010) Topographic effects on solar radiation distribution in mountainous watersheds and their influence on reference evapotranspiration estimates at watershed scale. *Hydrology and Earth System Sciences*, 14, 2479–2494. https://doi.org/10.5194/hess-14-2479-2010

Bertrand, C., Vanderveken, G. and Journée, M. (2015) Evaluation of decomposition models of various complexity to estimate the direct solar irradiance over Belgium. *Renewable Energy*, 74, 618–626. https://doi.org/10.1016/j.renene.2014.08.042

Beyer, H.G., Costanzo, C. and Heinemann, D. (1996) Modifications of the Heliosat procedure for irradiance estimates from satellite images. *Solar Energy*, 56(3), 207–212.

Bohn, T.J., Livneh, B., Oyler, J.W., Running, S.W., Nijssen, B. and Lettenmaier, D.P. (2013) Global evaluation of MTCLIM and related algorithms for forcing of ecological and hydrological models. *Agricultural and Forest Meteorology*, 176, 38–49. https://doi.org/10.1016/j.agrformet.2013.03

CAMS, 2019. *User Guide to the CAMS Radiation Service*. Available at: https://atmosphere.copernicus.eu/sites/default/files/2020-03/CAMS72_2018SC1_D72.4.3.1_2019_UserGuide_v1.1.pdf [Accessed 25 June 2020].

Cano, D., Monget, J.M., Albuisson, M., Guillard, H., Regas, N. and Wald, L. (1986) A method for the determination of the global solar radiation from meteorological satellite data. *Solar Energy*, 37(1), 31–39,1986.

Carrer, D., Roujean, J.-L. and Meurey, C. (2010) Comparing operational MSG/SEVIRI land surface albedo products from land SAF with ground measurements and MODIS. *IEEE Transactions on Geoscience and Remote Sensing*, 48(4), 1714–1728. https://doi.org/10.1109/TGRS.2009.2034530

Carrer, D., Ceamanos, X., Moparthy, S., Vincent, C., Freitas, S.C. and Trigo, I.F. (2019a) Satellite retrieval of downwelling shortwave surface flux and diffuse fraction under all sky conditions in the framework of the LSA SAF program (part 1: methodology). *Remote Sensing*, 11, 2532. https://doi.org/10.3390/rs11212532

Carrer, D., Moparthy, S., Vincent, C., Ceamanos, X., Freitas, S.C. and Trigo, I.F. (2019b) Satellite retrieval of downwelling shortwave surface flux and diffuse fraction under all sky conditions in the framework of the LSA SAF program (part 2: evaluation). *Remote Sensing*, 11, 2630. https://doi.org/10.3390/rs11222630

Ceamanos, X., Carrer, D. and Roujean, J.-L. (2014a) Improved retrieval of direct and diffuse downwelling surface shortwave flux in cloudless atmosphere using dynamic estimates of aerosol content and type: application to the LSA-SAF project. *Atmospheric Chemistry and Physics*, 14, 8209–8232. https://doi.org/10.5194/acp-14-8209-2014

Ceamanos, X., Carrer, D. and Roujean, J.-L. (2014b) An efficient approach to estimate the transmittance and reflectance of a mixture of aerosol components. *Atmospheric Research*, 137, 125–135. https://doi.org/10.1016/j.atmosres.2013.09.009

Chirici, G., Chiesi, M., Corona, P., Salvati, R., Papale, D., Fibbi, L., Sirca, C., Spano, D., Duce, P., Marras, S., Matteucci, G., Cescatti, A. and Maselli, F. (2016) Estimating daily forest carbon fluxes using a combination of ground and remotely sensed data. *Journal of Geophysical Research – Biogeosciences*, 121(2), 266–279. https://doi.org/10.1002/2015JG003019

Cristóbal, J. and Anderson, M.C. (2013) Validation of a Meteosat second generation solar radiation dataset over the northeastern Iberian Peninsula. *Hydrology and Earth System Sciences*, 17(1), 163–175. https://doi.org/10.5194/hess-17-163-2013

Demain, C., Journée, M. and Bertrand, C. (2013) Evaluation of different models to estimate the global solar radiation on inclined surfaces. *Renewable Energy*, 50, 710–721. https://doi.org/10.1016/j.renene.2012.07.031

Dozier, J. and Frew, J. (1990) Rapid calculation of terrain parameters for radiation modeling from digital elevation data. *IEEE Transactions on Geoscience and Remote Sensing*, 28(5), 963–969.

Driemel, A., Augustine, J., Behrens, K., Colle, S., Cox, C., Cuevas-Agulló, E., Denn, F.M., Duprat, T., Fukuda, M., Grobe, H., Haeffelin, M., Hodges, G., Hyett, N., Ijima, O., Kallis, A., Knap, W., Kustov, V., Long, C.N., Longenecker, D., Lupi, A., Maturilli, M., Mimouni, M., Ntsangwane, L., Ogihara, H., Olano, X., Olefs, M., Omori, M., Passamani, L., Pereira, E.B., Schmithüsen, H., Schumacher, S., Sieger, R., Tamlyn, J., Vogt, R., Vuilleumier, L., Xia, X., Ohmura, A. and König-Langlo, G. (2018) Baseline surface radiation network (BSRN): structure and data description (1992–2017). *Earth System Science Data*, 10, 1491–1501. https://doi.org/10.5194/essd-10-1491-2018

Fibbi, L., Chiesi, M., Moriondo, M., Bindi, M., Chirici, G., Papale, D., Gozzini, B. and Maselli, F. (2016) Correction of a

1 km daily rainfall dataset for modelling forest ecosystem processes in Italy. *Meteorological Applications*, 23(2), 294–303. https://doi.org/10.1002/met.1554

Flint, A.L. and Childs, S.W. (1987) Calculation of solar radiation in mountainous terrain. *Agricultural and Forest Meteorology*, 40, 233–249.

Geiger, B., Carrer, D., Franchistéguy, L., Roujean, J.-L. and Meurey, C. (2008a) Land surface albedo derived on a daily basis from Meteosat second generation observations. *IEEE Transactions on Geoscience and Remote Sensing*, 46(11), 3841–3856. https://doi.org/10.1109/TGRS.2008.2001798

Geiger, B., Meurey, C., Lajas, D., Franchistéguy, L., Carrer, D. and Roujean, J.-L. (2008b) Near real-time provision of downwelling shortwave radiation estimates derived from satellite observations. *Meteorological Applications*, 15(3), 411–420. https://doi.org/10.1002/met.84

Haurant, P., Muselli, M., Pillot, B. and Oberti, P. (2012) Disaggregation of satellite derived irradiance maps: evaluation of the process and application to Corsica. *Solar Energy*, 86(11), 3168–3182. https://doi.org/10.1016/j.solener.2012.08.010

Haylock, M.R., Hofstra, N., Klein Tank, A.M.G., Klok, E.J., Jones, P. D. and New, M. (2008) A European daily high-resolution gridded data set of surface temperature and precipitation for 1950–2006. *Journal of Geophysical Research (Atmospheres)*, 113, D20119. https://doi.org/10.1029/2008JD010201

Huang, P. and Zhao, W. (2017) The preliminary investigation on the uncertainties associated with surface solar radiation estimation in mountainous areas. *IEEE Geoscience and Remote Sensing Letters*, 14(7), 1071–1075. https://doi.org/10.1109/LGRS.2017.2696973

Iqbal, M. (1983) *An Introduction to Solar Radiation*. Toronto: Academic Press, 390 pp.

Journée, M. and Bertrand, C. (2010) Improving the spatio-temporal distribution of surface solar radiation data by merging ground and satellite measurements. *Remote Sensing of Environment*, 114(11), 2692–2704. https://doi.org/10.1016/j.rse.2010.06.010

Kang-tsung, C. and Bor-wen, T. (1991) The effect of DEM resolution on slope and aspect mapping. *Cartography and Geographic Information Systems*, 18(1), 69–77. https://doi.org/10.1559/152304091783805626

Laiti, L., Giovannini, L., Zardi, D., Belluardo, G. and Moser, D. (2018) Estimating hourly beam and diffuse solar radiation in an Alpine Valley: a critical assessment of decomposition models. *Atmosphere*, 9, 117. https://doi.org/10.3390/atmos9040117

Lefèvre, M., Oumbe, A., Blanc, P., Espinar, B., Gschwind, B., Qu, Z., Wald, L., Schroedter-Homscheidt, M., Hoyer-Klick, C., Arola, A., Benedetti, A., Kaiser, J.W. and Morcrette, J.-J. (2013) McClear: a new model estimating downwelling solar radiation at ground level in clear-sky conditions. *Atmospheric Measurement Techniques*, 6, 2403–2418. https://doi.org/10.5194/amt-6-2403-2013

Marchand, M., Lefèvre, M., Saboret, L., Wey, E. and Wald, L. (2019) Verifying the spatial consistency of the CAMS radiation service and HelioClim-3 satellite-derived databases of solar radiation using a dense network of measuring stations: the case of The Netherlands. *Advances in Science and Research*, 16, 103–111. https://doi.org/10.5194/asr-16-103-2019

Maselli, F., Pasqui, M., Chirici, G., Chiesi, M., Fibbi, L., Salvati, R. and Corona, P. (2012) Modeling primary production using a 1 km daily meteorological data set. *Climate Research*, 54, 271–285. https://doi.org/10.3354/cr01121

Michalsky, J.J. (1988) The astronomical Almanac's algorithm for approximate solar position (1950–2050). *Solar Energy*, 40(3), 227–235. https://doi.org/10.3354/cr01121

Moreno, A., Gilabert, M.A., Camacho, F. and Martínez, B. (2013) Validation of daily global solar irradiation images from MSG over Spain. *Renewable Energy*, 60, 332–342. https://doi.org/10.1016/j.renene.2013.05.019

Oumbe, A., Blanc, P., Ranchin, T., Schroedter-Homscheidt, M. and Wald, L. (2009) A new method for estimating solar energy resource. In *Proceedings of the ISRSE 33, Stresa, Italy, 4–9 May 2009*. Ispra: Joint Research Center, paper 773.

Padovan, A. and Del Col, D. (2010) Measurement and modeling of solar irradiance components on horizontal and tilted planes. *Solar Energy*, 84(12), 2068–2084. https://doi.org/10.1016/j.solener.2010.09.009

Qu, Z., Oumbe, A., Blanc, P., Espinar, B., Gesell, G., Gschwind, B., Klüser, L., Lefèvre, M., Saboret, L., Schroedter-Homscheidt, M. and Wald, L. (2017) Fast radiative transfer parameterisation for assessing the surface solar irradiance: the Heliosat-4 method. *Meteorologische Zeitschrift*, 26(1), 33–57. https://doi.org/10.1127/metz/2016/0781

Reindl, D.T., Beckman, W.A. and Duffie, J.A. (1990) Diffuse fraction correlations. *Solar Energy*, 45(1), 1–7. https://doi.org/10.1016/0038-092X(90)90060-P

Rigollier, C., Lefèvre, M. and Wald, L. (2004) The method Heliosat-2 for deriving short-wave solar radiation from satellite images. *Solar Energy*, 77(2), 159–169. https://doi.org/10.1016/j.solener.2004.04.017

Ruiz-Arias, J.A., Cebecauer, T., Tovar-Pescador, J. and Šúri, M. (2010) Spatial disaggregation of satellite-derived irradiance using a high-resolution digital elevation model. *Solar Energy*, 84(9), 1644–1657. https://doi.org/10.1016/j.solener.2010.06.002

Ruiz-Arias, J.A., Pozo-Vázquez, D., Lara-Fanego, V., Santos-Alamillos, F.J. and Tovar-Pescador, J. (2011) A high-resolution topographic correction method for clear-sky solar irradiance derived with a numerical weather prediction model. *Journal of Applied Meteorology and Climatology*, 50(12), 2460–2472. https://doi.org/10.1175/2011JAMC2571.1

Schroedter-Homscheidt, M., Betcke, J., Breitkreuz, H., Hammer, A., Heinnemann, D., Petrack S., Holzer-Popp, T. and Wald, L. (2006) Energy-specific solar radiation data from MSG: the Heliosat-3 Project. In *Proceedings of 3rd MSG RAO Workshop, 15 Jun 2006*, Helsinki, Finland: ESA, SP-619, 52–57 ESA Publications Division, The Netherlands.

Sengupta, M., Habte, A., Kurtz, S., Dobos, A., Wilbert, S., Lorenz, E., Stoffel, T., Rennè, D., Gueymard, C., Myers, D., Wilcox, S., Blanc, P. and Perez, R. (2015) *Best Practices Handbook for the Collection and Use of Solar Resource Data for Solar Energy Applications*. Technical Report NREL/TP-5D00-63112. Golden, CO: National Renewable Energy Laboratory.

Skartveit, A., Olseth, J.A. and Tuff, M.E. (1998) An hourly diffuse fraction model with correction for variability and surface albedo. *Solar Energy*, 63(3), 173–183. https://doi.org/10.1016/S0038-092X(98)00067-X

Suehrcke, H., Bowden, R.S. and Hollands, K.G.T. (2013) Relationship between sunshine duration and solar radiation. *Solar Energy*, 92, 160–171. https://doi.org/10.1016/j.solener.2013.02.026

Tarpley, J.D. (1979) Estimating incident solar radiation at the surface from geostationary satellite data. *Journal of Applied Meteorology*, 18(9), 1172–1181.

Thornton, P.E., Running, S.W. and White, M.A. et al. (1997) Generating surfaces of daily meteorological variables over large regions of complex terrain. *Journal of Hydrology*, 190(3–4), 214–251. https://doi.org/10.1016/S0022-1694(96)03128-9

Thornton, P.E. and Running, S.W. et al. (1999) An improved algorithm for estimating incident daily solar radiation from measurements of temperature, humidity, and precipitation. *Agriculture and Forest Meteorology*, 93(4), 211–228. https://doi.org/10.1016/S0168-1923(98)00126-9

Thornton, P.E., Hasenauer, H. and White, M.A. et al. (2000) Simultaneous estimation of daily solar radiation and humidity from observed temperature and precipitation: an application over complex terrain in Austria. *Agricultural and Forest Meteorology*, 104(4), 255–271. https://doi.org/10.1016/S0168-1923(00)00170-2

Trigo, I.F., Dacamara, C.C., Viterbo, P., Roujean, J.-L., Olesen, F., Barroso, C., Camacho-de-Coca, F., Carrer, D., Freitas, S.C., García-Haro, J., Geiger, B., Gellens-Meulenberghs, F., Ghilain, N., Meliá, J., Pessanha, L., Siljamo, N. and Arboleda, A. (2011) The satellite application Facility for Land Surface Analysis. *International Journal of Remote Sensing*, 32(10), 2725–2744. https://doi.org/10.1080/01431161003743199

Urraca, R., Gracia-Amillo, A.M., Koubli, E., Huld, T., Trentmann, J., Riihelä, A., Lindfors, A.V., Palmer, D., Gottschalg, R. and Antonanzas-Torres, F. (2017) Extensive validation of CM SAF surface radiation products over Europe. *Remote Sensing of Environment*, 199, 171–186. https://doi.org/10.1016/j.rse.2017.07.013

Wahab, M.A., El-Metwally, M., Hassan, R., Lefèvre, M., Oumbe, A. and Wald, L. (2010) Assessing surface solar irradiance and its longterm variations in the northern Africa desert climate using Meteosat images. *International Journal of Remote Sensing*, 31 (1), 261–280. https://doi.org/10.1080/01431160902882645

Wild, M. (2016) Decadal changes in radiative fluxes at land and ocean surfaces and their relevance for global warming. *WIREs Climate Change*, 7(1), 91–107. https://doi.org/10.1002/wcc.372

How to cite this article: Fibbi L, Maselli F, Pieri M. Improved estimation of global solar radiation over rugged terrains by the disaggregation of Satellite Applications Facility on Land Surface Analysis data (LSA SAF). *Meteorol Appl*. 2020;27:e1940. https://doi.org/10.1002/met.1940